Large improvement of CNT yarn electrical conductivity by varying chemical doping and annealing treatment

Yoann Dini, Denis Rouchon, Jérôme Faure-Vincent, Jean Dijon

Large improvement of CNT yarn electrical conductivity by chemical doping, annealing treatment and combination of both

Yoann Dini [a], *Denis Rouchon* [b], *Jérôme Faure-Vincent* [c*], *Jean Dijon* [a]

[a] Univ Grenoble-Alpes, CEA, LITEN, DTNM, F-38000 Grenoble, France

[b] Univ Grenoble-Alpes, CEA, LETI, DPFT, F-38000 Grenoble, France

[c] Univ Grenoble-Alpes, CEA, CNRS, INAC-SyMMES, F-38000 Grenoble, France

*Corresponding author. Tel: +33 4 38783409 E-mail: jerome.faure-vincent@cea.fr

Abstract

High conductive carbon nanotube (CNT) yarns are a near challenge to be an alternative to metal in electrical wiring. In this work, we largely improve carbon nanotube yarn electrical conductivity by chemical doping, annealing treatments (above 2000 °C) and combination of both. We present a new efficient CNT p-type dopant based on platinum chloride IV. It decreases the resistivity by a factor of 3 and is stable over half a year. The annealing treatments above 2000 °C dramatically improve the CNT structural quality by a decade. In addition, we show that the CNT yarn electrical resistivity decreases linearly with the CNT structural quality increase and we report the world record resistivity for an undoped CNT yarn spun from CNT array (0.76 mΩ.cm). We reveal that the CNT structural quality is not the only factor needed to reach high electrical conductivities. The increase in CNT structural quality significantly improves the doping efficiency by a factor of 2. By systematic measurements of the CNT yarn and web resistance from 3 K to 300 K, we are able to explain the influence of the doping, annealing, compaction and CNT length on the electrical charge transport.

1 Introduction

Carbon nanotubes (CNTs) are known to have high electrical and thermal properties as well as excellent mechanical properties and a low density [1–3]. Individual carbon nanotubes (CNTs) possess very low electrical resistivities as low as 5.1 μΩ.cm for a 9.1 nm diameter multi wall CNT [4] and typically between 1 and 10 μΩ.cm [5]. The assembly of CNTs into a yarn is therefore a possible alternative to metallic wires in aerospace [6] and wearable textile [1]. However, when CNTs are macroscopically assembled into yarns, the final resistivity (usually between 12 – 1000 μΩ.cm [7]) is higher than that of individual CNTs. In our previous work we concluded that the intrinsic CNT performances limit the conductivity of CNT yarns spun from CNT arrays [7]. The aim of this work is to drastically decrease the resistivity of CNT yarn spun from CNT arrays by chemical doping, annealing treatment at very high temperatures (above 2000 °C) and combination of both. In the meantime, this work focuses on measuring CNT yarn resistance variations as a function of the temperature (3 K - 300 K) to bring out the full CNT yarn electrical transport.

In room conditions, pristine carbon nanotubes are generally p-type semiconductors [8]. P-type dopants like $AuCl_3$ [9], I_2 [10], or acids such as HNO_3 [11] and H_2SO_4 [12] have already been reported as a way to decrease CNT material resistivities. The doping efficiencies (pristine sample resistance divided by its resistance after doping) of acids are usually limited around 2 [12,13]. However, higher doping efficiencies around 3 are reported for iodine doped CNT sheets [14,15] and $AuCl_3$ doped CNT yarn draw from array [16]. Apart from the conductivity improvement, long term time stability is also a critical parameter for any electrical application. It is known that iodine [17] or $AuCl_3$ [18] doping are deteriorated over rather short time but, unfortunately, most publications on doping do not mention this important phenomenon. In this work, we present a new patented metallic chloride dopant called platinum chloride IV ($PtCl_4$) [19] (patent: US20180142346) that allows both high doping efficiency and very long term time stability. We also investigate how this new dopant impacts the electronic transport in the CNT materials.

The second way to decrease CNT yarn conductivity is to increase the CNT structural quality by annealing treatments. However, the CNT structural quality is highly dependent on the annealing temperature. Low annealing temperatures do not allow to significantly increase the CNT structural quality as attested by Yang et al. [21]. They showed that their CNT yarn G over D band intensity

ratio (I_G/I_D) of the Raman spectra (parameter characteristic of the CNT structural quality) is only increased by 1.6 after a 900 °C treatment. Very high temperatures are needed to decrease the number of CNT defects. Yamamoto et al. [22] and Mattia et al. [20] showed that the annealing temperature needs to be higher than 2000 °C in order to drastically increase the CNT structural quality. Yamamoto et al. [22] report that the CNT's I_G/I_D is increased by a factor of 10 after a 1 hour annealing time at 2600 °C. Calculations also show that at those high temperatures, CNT defects such as Stone-Wales defects can be healed [23]. This is the reason why, in this work, we are using annealing temperatures above 2000 °C and as high as 2450 °C. The number of publications on CNT yarns annealed above 2000 °C is limited. Recently, Niven et al. [24] showed that after 2.5 hours at 2700 °C the CNT yarn drawn from array I_G/I_D was increased by a factor of 4 and its resistivity was decreased from 6.7 mΩ.cm to 2.9 mΩ.cm. Our work is consistent with their findings but go further by studying the impact on the CNT yarn electrical transport of three different temperatures (2010 °C, 2250 °C, and 2450°C) and for much longer treatment duration (up to 72 hours). In addition, we are reporting much better I_G/I_D improvement and much lower resistivities (below the 1 mΩ.cm resistivity limitation faced by all CNT yarns draw from arrays [7]). We also investigate the influence of doping an annealed CNT yarn and we show that the annealing efficiency is cumulative with that of doping.

Finally, based on our systematic electrical transport studies of the treated CNT yarns in this work and our previous work [7], we are able to clearly identify the factors (CNT interconnections, CNT structural quality, doping) affecting the electronic transport of CNT assemblies such as yarns and webs.

2 Experimental Section

2.1 Yarn production and characterization

CNT arrays are produced by a low pressure fixed-catalyst hot filament chemical vapor deposition (CVD) reactor (see Dini et al. [7] for more details). The substrate is made of a silicon wafer bearing a silica-based layer deposited by Atomic Layer Deposition. A 1.5 nm iron catalyst layer is deposited on the substrate by electron beam evaporation. The growth temperature is around 630 °C and the precursor gas is acetylene mixed with hydrogen and helium. Produced CNTs have, on average, 6 walls and a diameter of around 7 nm (see Figure 1a). CNT webs and yarns are spun from 200 µm high CNT arrays. In our previous work [7], we extensively studied the CNT web morphology and we concluded that our CNT webs are made of individualized CNT bundles (see figure 1b and 1c) of 23 nm in diameter on average and made on average of 7 individual CNTs. The CNT yarn diameters range from 8 to 15 µm (see Figure 1d). In order to allow a comparison between CNT yarns, all CNT yarns used in this work have the same twist angle of 20° ± 3°. The impact of the twist angle on the CNT yarn electrical transport was extensively studied in our previous work [7].

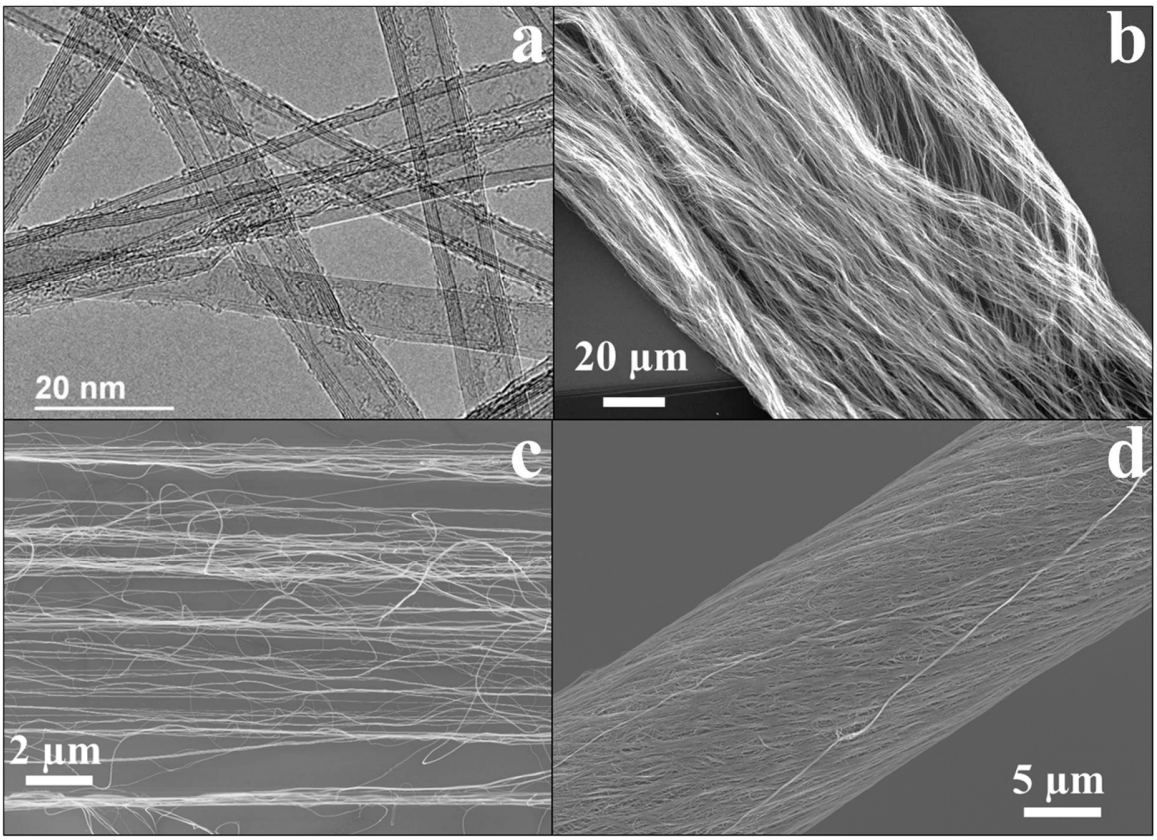

Figure 1 : As grown CNTs high resolution transmission electron microscope image (a), CNT web scanning electron microscope (SEM) images at low magnification (b) and high magnification (c), CNT yarn SEM image (d).

With our CNT growth process, CNT arrays as well as webs and yarns have a very low content of amorphous carbon (lower than 1 wt%) and a weight percent of iron catalyst close to 0 wt% (see thermogravimetric analysis of the CNTs in supplementary data S1). Scanning electron microscopy (SEM) images are performed with a high resolution Zeiss Ultra 55 microscope to measure the CNT yarn diameters and CNT array heights. Those measurements are also confirmed by optical microscopy.

Prior to any electrical measurements, CNT webs and yarns are laid on a silicon wafer bearing a 500 nm insulating silica layer. CNT web electrodes are deposited by gold thermal evaporation. CNT yarn electrodes are silver ink printed. Electrical measurements were performed by using the standard four probe sensing method through the combination of a Keithley 220 current source and two Keithley 6512 electrometers. Prior to any resistance measurements at low temperature, samples are pumped under primary vacuum overnight. The temperature was varied from 3 K up to 350 K

using a dynamic helium flow cryostat Oxford Instruments CF 1200 D. More details on the fabrication process and sample characterizations can be found in our previous work [7]. Raman spectroscopy is a powerful technique that can be used to characterize the order of carbon nanotubes structures via G (1580 cm^{-1}) and D (around 1360 cm^{-1}) vibration bands The G over D band intensity ratio of the Raman spectra (I_G/I_D) gives valuable information on the crystallinity (graphitization degree) and the purity of carbon nanotube materials [25]. Raman spectra were recorded in the backscattering geometry using a Renishaw Raman spectrometer. Light was focused onto the sample surface using a 100 x (0.9 NA) short working objective lens, resulting in a spot diameter around 0.8 μm. The excitation wavelength was 532 nm with a typical laser power of ~0.5 mW to avoid any heating of the CNT yarns. The spectral lines used for the analysis were fitted with Lorentzian functions in order to increase accuracy.

2.2 Doping Treatment

The dopant agent used in this work is platinum chloride IV ($PtCl_4$). It is purchased from Sigma-Aldrich and has a purity of 99.9 wt%. The $PtCl_4$ is solubilized in pure acetonitrile with a 1 mmol/l concentration. Two techniques are used to dope our carbon nanotube samples. The first one is a dipping technique. We dipped the CNT web into the dopant solution. After 5 minutes we take it out, we apply a twist to densify it into a yarn and we let it dry for one hour in room conditions (air, atmospheric pressure and room temperature). Afterwards, electrodes are silver ink printed. The second technique is a drop casting method. CNT webs and yarns, connected to their electrodes, are put on a hot plate at 100 °C. Dopant solution droplets are deposited on the hot sample surface. Due to the low boiling point of acetonitrile (82 °C), the solvent evaporates and the doped sample is dried. Each new droplet is deposited after the previous one has totally been evaporated. A total of 10 dopant solution droplets are deposited on the samples.

2.3 Annealing treatment

CNT yarns are annealed using a unique technique. We modified our hot filament CVD reactor. For a typical use, we can power up to 1000 W through 10 graphitic carbon filaments. Reactor design details are given in our previous work [7]. In order to perform high temperature annealing

treatments, we are using one single graphitic carbon filament powered up to a maximum of 400 W. The carbon nanotube yarn is tightly wrapped around the carbon filament to ensure excellent thermal contact (see supplementary data S2).

The carbon filament used in this work are purchased from Entegris and are 9.2 cm long and 0.5 mm in diameter. The filament is placed inside our low pressure CVD reactor. In this work all the annealing treatments are performed under secondary vacuum (below 10^{-4} Pa). Due to the voltage limitation of the power source (40 V) and the resistance of the carbon filament it is not possible to apply more than 400 W on a single filament. The annealing time is tunable and the maximum annealing time is 72 hours. It is very hard to measure the temperature of one filament because of its small diameter. Pyrometer cannot work in this case and largely underestimates the filament temperature due to the cold background. Nevertheless, under vacuum, by using the Stefan–Boltzmann law we can easily calculate the carbon filament temperature based on its resistance and the delivered electrical power. The evolution of the carbon filament resistance with its temperature [26] and its emissivity are given by the manufacturer Entegris. The calculated filament temperature as function of the power is given in Figure 2. In this study, we are using three different powers: 200 W, 300 W and 400 W corresponding respectively to 2010 °C, 2250°C and 2440 °C.

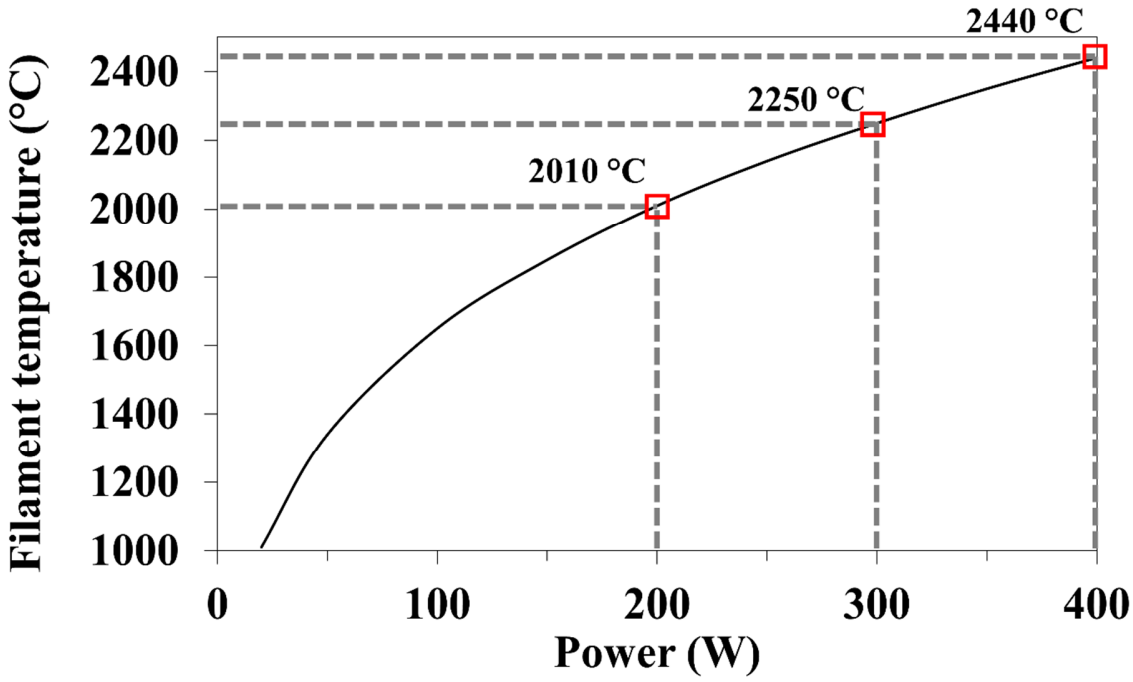

Figure 2: Calculated carbon filament temperature as function of the power input

3 Results and discussion

In the following section, the decrease of the CNT web and yarn resistance induced by the doping treatment, is estimated by the improvement factor (IF) defined as the pristine resistance divided by the doped resistance measured in room conditions (see equation 1).

$$Improvement\ Factor\ (IF) = \frac{R_{before\ doping}}{R_{after\ doping}} \quad (1)$$

The CNT material electrical transport will be analyzed by using both a parameter called resistance ratio and the reduced activation energy (W). The resistance ratio is defined as the ratio of the CNT material resistance at 3 K over its resistance at 300 K. The reduced activation energy W is defined as [27,28]:

$$W(T) = -\frac{d\ln(\rho(T))}{d\ln(T)} \quad (2)$$

where ρ is the electrical resistivity and T the temperature.

3.1 $PtCl_4$ doping

In this work, we are using platinum chloride IV ($PtCl_4$) as a CNT p-type dopant. Similarly to other metallic chlorides like $AuCl_3$ [29], $FeCl_3$ [30] or $CuCl_2$ [31], $PtCl_4$ adsorbate to the carbon nanotube surface inducing a hole charge transfer from the $PtCl_4$ to the CNT. Transmission electron microscope (TEM) images of $PtCl_4$ dopant structure on graphene explaining its good stability is presented in supplementary information S3-1 and S3-2. Information concerning $PtCl_4$ doping mechanism on CNTs are also detailed in previous works of our team by Liang et al [19,32].

Two methods are used to dope our samples: dipping and drop casting. More details on these two methods are given in the experimental section. The drop casting method was applied on both CNT yarns and webs. The G band upshifts in the doped CNT web and yarn Raman spectra (see Figure 3a and b) confirm the p-type doping of $PtCl_4$. The G band upshift is higher for the doped CNT web than the doped CNT yarn indicating that the doping efficiency is better for the CNT web [33]. This result is consistent with the electrical measurements: the best improvement factor 2.8 is obtained by doping a CNT web (see Figure 3c). Its resistance is decreased by almost a factor of 3 and the improvement is very stable over time (see figure 3d), the resistance only increases by 15 % over half a year. These results prove that $PtCl_4$ is an efficient CNT dopant [34]. However, the

improvement factor for a drop casted CNT yarn is poorer (1.7, see Figure 3c). This lower performance can be explained by the difference of CNT organization between the CNT yarn and the CNT web. CNT webs are made of a 2D network of individualized CNT bundles [7] (see Figure 1.b and 1c), whereas CNT bundles are tightly packed together in CNT yarns. Hence, due to the yarn compaction, it is harder for the dopant to reach all the CNT bundles in a yarn than in a web. The dopant will probably stay in the yarn outer rim. In order to allow the dopant to reach all the CNT bundles, we dipped a CNT web in the doping solution, then put it out and twisted it (dipping method). However, this last method show even poorer results (improvement factor of 1.5, see Figure 3c) than the drop casting method. This efficiency difference indicates that the dipping method deposits less dopant than the drop casting one. A possible explanation is that, in the dipping method, there are two mechanisms in competition: the adsorption of dopant onto the CNT bundle surface and the dopant staying in solution. Whereas, in the drop casting method, due to the solvent evaporation, there is only one mechanism: all the dopant is forced to stay onto the CNT yarn.

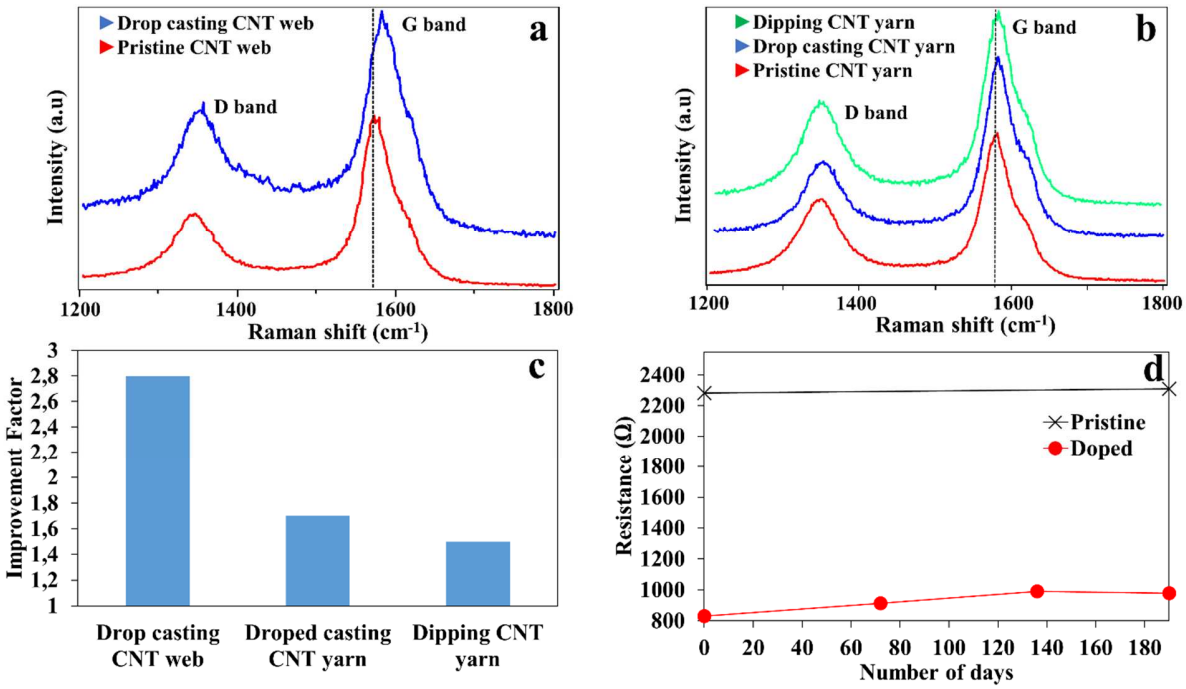

Figure 3: Raman spectra of a pristine (blue) and a drop casting (red) CNT web (a). Raman spectra of a pristine (red), dipped (green) and drop casting (red) CNT yarn (b). Improvement factor (IF) as a function of techniques and samples (c), Resistance time stability of a doped CNT web (d).

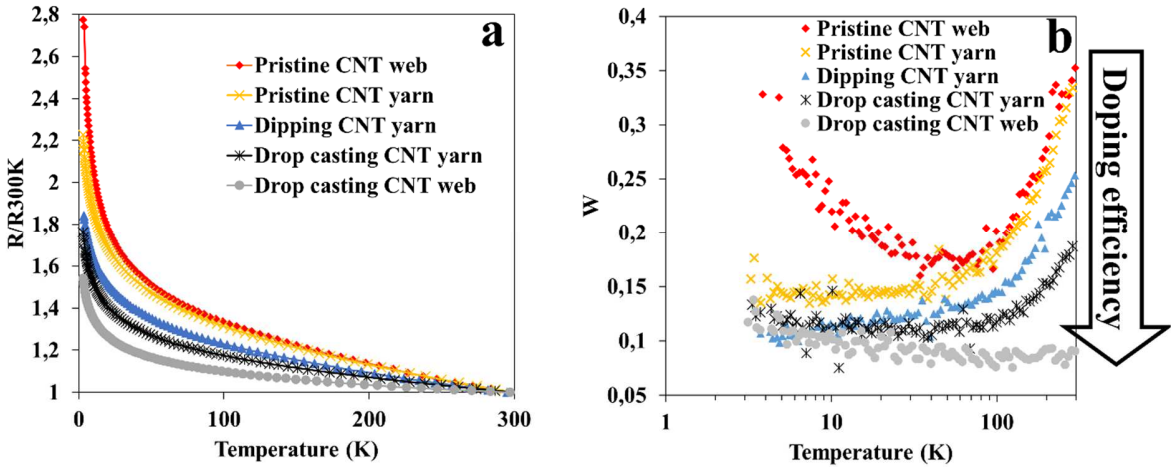

Figure 4: Resistance of doped samples versus temperature (a) and their reduced activation energy (W) as function of the temperature (b)

The electronic transport in pristine CNT yarn and web present a semiconducting behavior, i.e. the resistance decreases as the temperature increases (Figure 4a). Doped CNT yarns and webs also show a similar electronic transport but have a smaller resistance ratio (between 1.5 and 1.8) than the pristine CNT yarn and web (between 2.2 and 2.8). As a consequence, the doping treatment dramatically reduces the semiconducting behavior of our CNT materials. The resistance ratio decreases as the improvement factor increases. For example, the drop casting CNT web resistance ratio (1.5) is smaller than that of the drop casting doped CNT yarn (1.7) which is smaller than that of the dipped doped CNT yarn (1.8).

Similarly, the doping impact on the semiconducting behavior is also supported by the reduced activation energy curves (Figure 4b). On the whole temperature range (3 K to 300 K), the reduced activation energies of the doped samples are lower than those of the pristine ones. This indicates that the electrical transport in CNTs is facilitated by the doping treatment (diminution of the semiconducting behavior for both yarns and webs). Particularly, the decrease of the reduced activation energy (W) slope above 70 K is linked to the improvement factor (see Figure 4b and supplementary data S4). Thus, the W slope analysis above 70 K is a useful and complementary tool to monitor the doping efficiency.

3.2 Annealing treatment

3.2.1 CNT structural quality and CNT yarn resistivity

Annealing treatment at high temperature is very efficient to improve the carbon nanotube structural quality [35]. In this work, CNT yarns were annealed at temperatures above 2000°C. Three annealing temperatures were performed: 2010°C, 2250°C and 2440 °C for various durations up to 72 hours. Experimental details on the annealing treatment are given in the experimental section. In figure 5, SEM images of a pristine yarn (Figure 5a-c) and the CNT yarn annealed at 2250 °C for 8 hours (Figure 5d-f) reveal that the treatment preserves the CNT yarn physical integrity. Interestingly, we noticed that annealed CNT yarns handling did not look different from the pristine ones. Qualitatively, mechanical properties are not altered by the annealing treatment. This behavior is consistent with Di et al. works [36] where they measured that the CNT yarn drawn from array tensile strength was only decreased by 10% after a 2000 °C annealing treatment. After the annealing treatment, the yarn is denser and CNTs are better aligned.

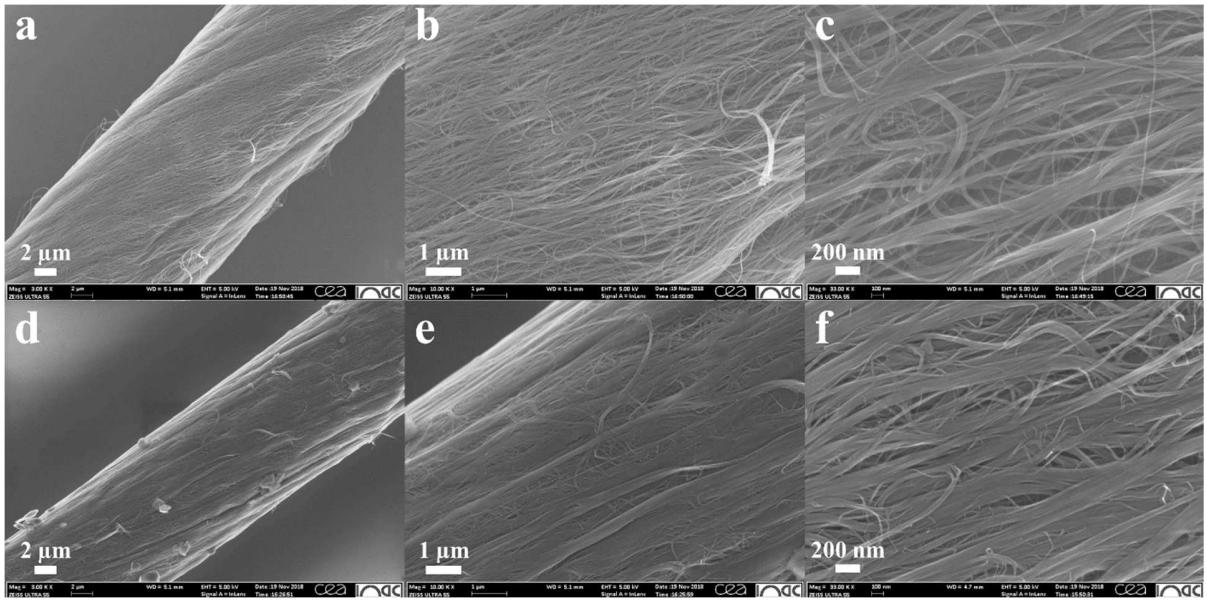

Figure 5: SEM images at three magnifications of a pristine yarn (a, b, c) and a CNT yarn annealed at 2250°C for 8 hours (d, e, f)

The CNT structural quality is measured by Raman spectroscopy. We are particularly interested in the intensity ratio of the G over D bands (I_G/I_D) that is proved to be correlated to a density of defects in the carbon nanotube structure [37–39]. By Raman spectroscopy we investigate the influence of

the annealing temperature and duration on the carbon nanotube structural quality (I_G/I_D). All annealed and pristine CNT yarns Raman spectra have been measured and are reported in Figure 6a. For annealed samples, we did not notice any changes in the Raman spectra along the yarn indicating that the annealing treatment was uniform (see supplementary data S5). Consistently with the literature [22,24,40], there is a dramatic increase of I_G/I_D with the annealing treatment. The CNT structural quality is drastically improved by annealing temperatures above 2000 °C. The best structural quality is obtained by annealing CNT yarn at 2250°C for 11 hours: the I_G/I_D ratio is increased by a decade, going from 1.6 to 15. Based on the thermogravimetric analysis of our CNT (See supplementary data S1), the I_G/I_D improvement is not due to CNT purification. In figure 6b, we present the evolution of I_G/I_D as a function of the annealing time and the three annealing temperatures (2010 °C, 2240 °C and 2440 °C).

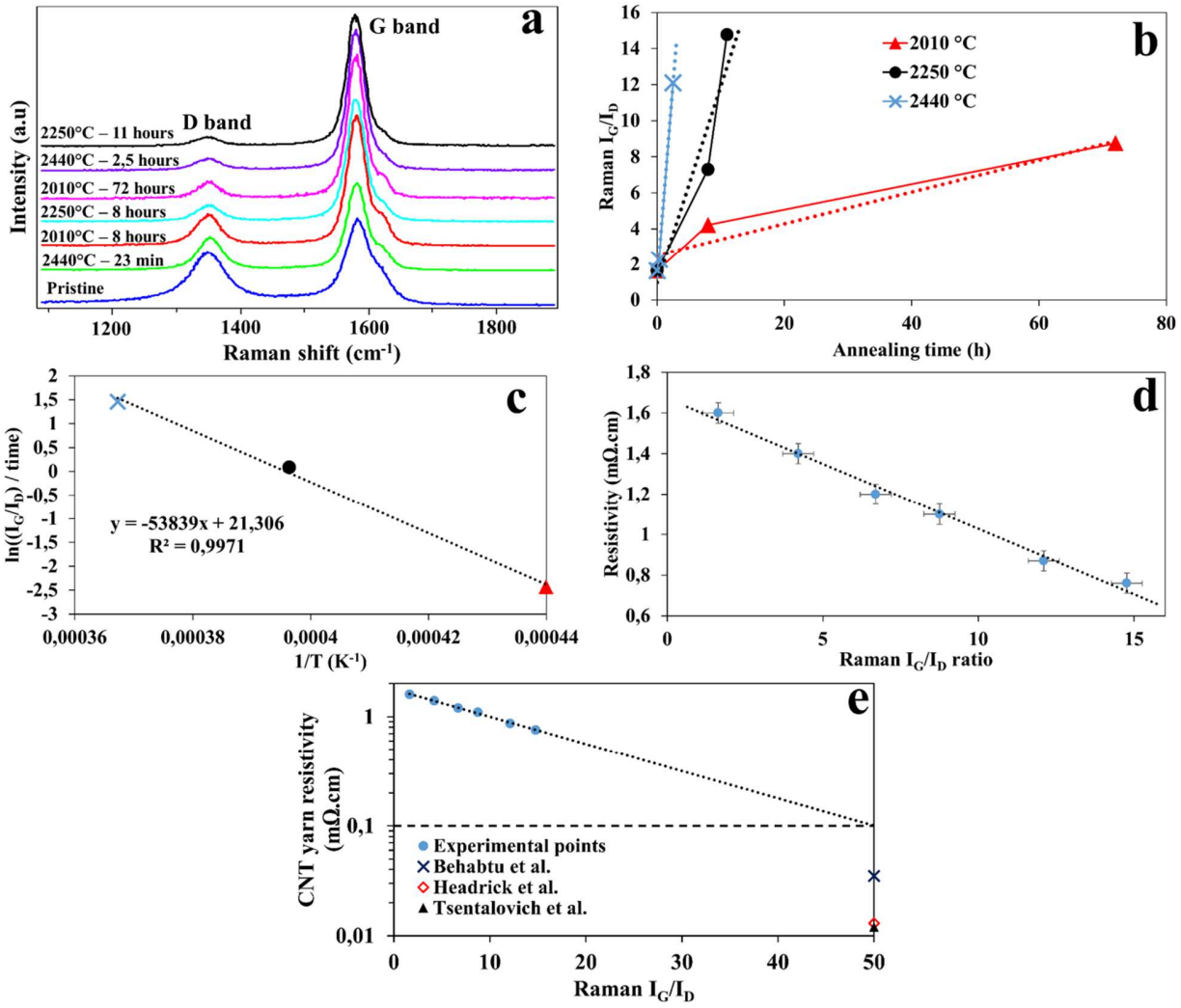

Figure 6: Raman spectra of pristine and annealed CNT yarns (a), CNT yarn I_G/I_D Raman spectra as a function of the annealing time and temperature (b), Arrhenius plot of data in b (c), annealed CNT yarn resistivities as a function of their I_G/I_D Raman ratio (d) and linear extrapolation of data in d to higher I_G/I_D and CNT yarn literature resistivities (e) : blue cross Behabtu et al.[41], red diamond Headrick et al.[42] and black triangle Tsentalovich et al. [43].

The I_G/I_D increase is very sensitive to the annealing temperature. The structural quality improvement is proportional to the annealing temperature. The higher the annealing temperature, the faster the CNT structural quality is improved. Due to the high temperature treatment, a chemical reaction is involved for CNT defects healing. As reported in the literature [44–46], the I_G/I_D can be used to monitor the evolution of CNT density defects as function of the treatment. Thus, the I_G/I_D slope as function of time (represented in dotted lines in Figure 6b) can be defined as a healing

reaction rate constant. We can clearly see in Figure 6b that the reaction rate constant increases with the annealing temperature increase (2010 °C, 2250 °C and 2440 °C). If we consider an Arrhenius plot of the healing reaction rate constant with the annealing temperature (Figure 6c), we observe that these two parameters are linearly correlated highlighting an activation energy for the CNT defect healing reaction. This measured activation energy correspond to the formation energy of defect in CNTs and is of 445 kJ/mol or 4.6eV. Interestingly, Stone-Wales defects in graphene and CNTs are reported in the literature to have a similar formation energy around 5 eV [47–49]. Our analysis of the I_G/I_D behavior with annealing temperature and duration suggests that Stone-Wales defects are healed by the annealing treatment. This work is the first one to experimentally measure the defect (Stone-Wales) formation energy for as-grown CNTs.

The annealing treatment considerably decreases the CNT yarn electrical resistivity in room conditions (air, atmospheric pressure and room temperature). The CNT structural quality improvement drops the CNT yarn resistivity by a factor of 2 going from 1.6 mΩ.cm for a pristine yarn to 0.76 mΩ.cm for a CNT yarn annealed at 2250 °C for 11 hours (see Figure 6d). This resistivity value is a new world record for undoped CNT yarns spun from CNT array that up to now are limited above 1 mΩ.cm [7]. This experiment proves that a good CNT structural quality is crucial to reach a high CNT yarn conductivity. Interestingly, if we extrapolate the linear relationship found between the CNT yarn resistivity and its I_G/I_D ratio (Figure 6d) to high values (up to 50 according to the litterature), we notice that the resistivity of CNT yarns spun from CNT arrays would still be limited above 100 µΩ.cm whereas the lowest wet spun CNT yarn resistivities are found to be as low as 12 µΩ.cm [41–43] (Figure 6e). Hence, the CNT structural quality is not the only parameter limiting the conduction in CNT yarns spun from CNT array. The use of multiwall CNTs or their organization into bundles could explain the lower performances of CNT yarns spun from arrays. Those possible limiting factors will be discussed in the last section.

3.2.2 Room conditions influence

Room conditions have no effect on a pristine CNT yarn conductivity but have a big impact on that of the annealed CNT yarn. Here, we only present the influence of room conditions on the CNT yarn annealed at 2250°C for 8 hours (Figure 7 a and b) but the other annealed CNT yarns are similarly impacted.

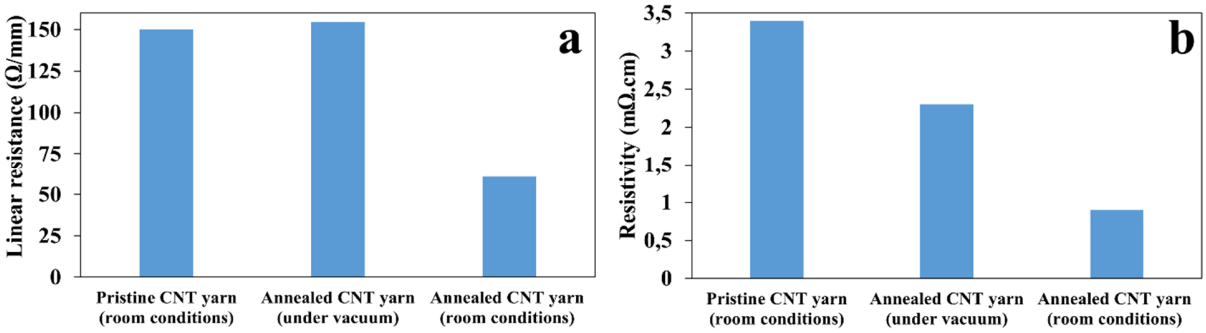

Figure 7: Linear resistances (a) and resistivities (b) of a pristine CNT yarn measured in room condition (17µm in diameter) and an annealed CNT yarn (13.8µm in diameter) both measured under vacuum and in room conditions.

The linear resistance of the annealed CNT yarn measured under vacuum is similar to that of the pristine CNT yarn (Figure 7a). As expected by the SEM images and the Raman spectra, this new result confirms that the annealing treatment does not deteriorate the CNT yarn. The annealing treatment densifies the CNT yarn, its diameter shrinks from 17 µm to 13.8 µm. This compaction is explained by Suenaga et al. [50] who observed by transmission electron microscopy that defects such as Stone-Wales defects induced kinks in CNTs. As a consequence, the reduction of CNT defects by the annealing treatment decreases the number of kinks leading to a CNT compaction. After 24 hours in room conditions, the annealed CNT yarn linear resistance and resistivity decrease by a factor 2.5 going respectively from 155 Ω/mm to 61 Ω/mm and from 2.3 to 0.9 mΩ.cm (see Figure 7b). This variation is totally reversible: when pumped under vacuum (below 10 Pa) overnight, the annealed CNT yarn resistivity shifts back from 0.9 to 2.3 mΩ.cm. The phenomenon takes several hours. This variation is due to a physisorption of O_2 and moisture to the CNT surface. The oxygen oxidizes CNTs and acts as a p-type dopant. It has already been observed that the CNT electrical transport is modified when exposed to air due to the presence of both moisture and oxygen [51–53]. The annealing treatment makes the CNT yarn more easily doped by oxygen. In order to understand this behavior, we analyze the electrical transport of the annealed CNT yarns by measuring their resistance as function of the temperature (from 3 K to 300 K, see Figure 8). Prior to this measurement we remind that samples are pumped under primary vacuum overnight to remove all residual air.

3.2.3 Annealed CNT yarn electrical transport

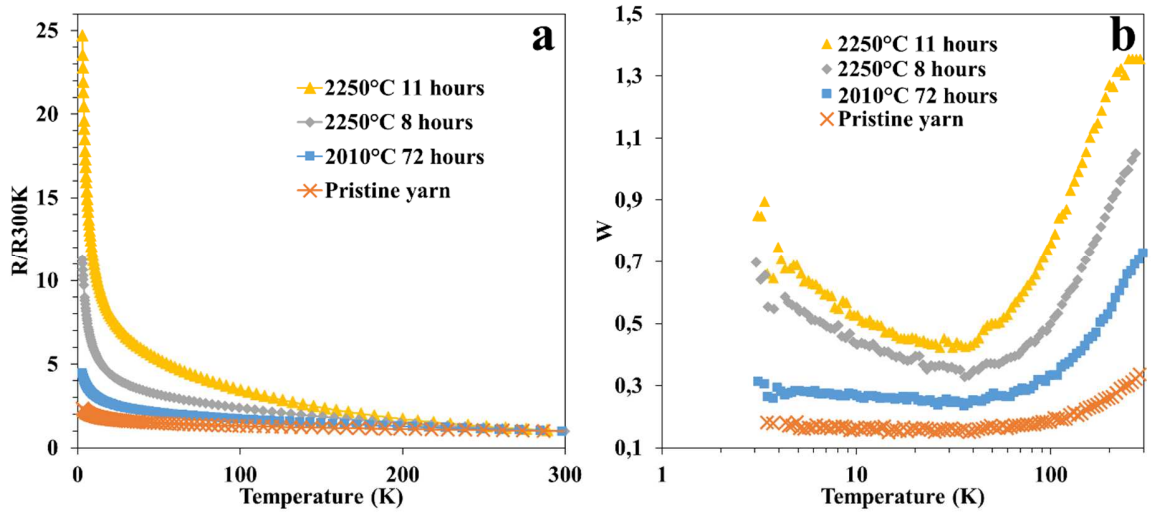

Figure 8: Resistance as a function of the temperature for annealed CNT yarns (a) and reduced activation energy (W) as a function of the temperature for annealed CNT yarns (b)

The annealing treatment strongly changes the CNT yarn electrical transport (see Figure 8a and b). A pristine CNT yarn has a resistance ratio of around 2 whereas a CNT yarn annealed at 2250°C for 11 hours has a ten times higher resistance ratio (24). The other annealed CNT yarns (72h at 2000°C and 8 h at 2250°C) also show a higher resistance ratio respectively 4.5 and 11. The CNT yarn resistance ratio and reduced activation energies (W) increase with the CNT structural quality improvement. Particularly, the W slope below 70 K becomes more negative shifting from the critical regime to the insulator regime (characteristic of the metal-insulator transition [54]). These last points show that by reducing the number of CNT defects, the CNT yarn semiconducting behavior is strengthened. Indeed, following Crespi et al. [55], part of the SC tubes becomes metallic (defect induced metallization). In addition, it is shown that, for multiwall CNTs, defects permit interwall electrical conduction [56] whereas only the two outer walls participate to the electrical transport in defect free multiwall CNTs [57]. Hence, in our pristine CNT yarn, defects connect the walls of our multiwall CNT allowing metallic conduction channels. This is why the pristine CNT yarn electrical transport is in the critical regime of the metal-insulator transition. After decreasing the number of defects by annealing, the density of available metallic walls decreases and the gap of the semiconducting CNTs widen. As a result the yarn electrical transport shifts from the critical regime to the insulating regime in the metal-insulator transition.

3.3 Combination of annealing and doping treatments

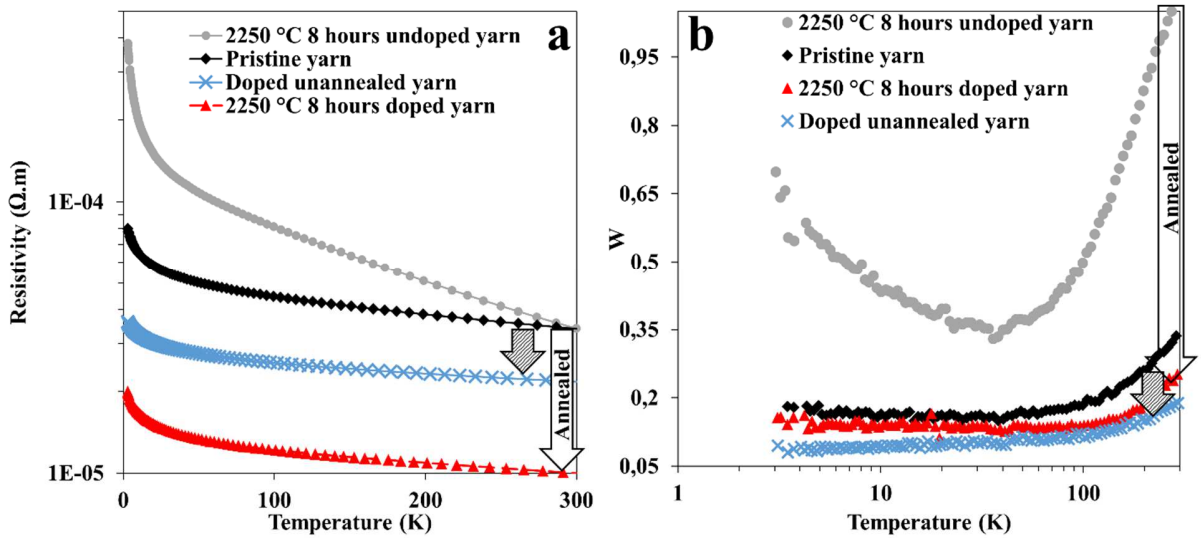

Figure 9: Resistivity (a) and reduced activation energy W (b) as function of the temperature for a pristine yarn (black diamond), undoped annealed yarn (grey circles), doped unannealed yarn (blue crosses), and doped annealed yarn (red triangle). The stripped arrow represents the resistivity decrease by doping a pristine yarn and the "annealed" arrow represents the resistivity decrease by doping an annealed yarn.

In order to fully characterize the CNT yarn semiconducting behavior induced by the annealing treatment, we are combining both annealing and doping treatments. Figure 9a presents the $PtCl_4$ doping influences on a pristine and an annealed (2250°C for 8 hours) CNT yarn electrical transport. We observe that the doping efficiency is highly better when the CNT yarn is annealed. As said in the doping section, a drop casting CNT yarn has its resistivity decreased by a factor of 1.7 (stripped arrow). Using the same doping condition, doping an annealed CNT yarn decreases its resistivity from 3.4 mΩ.cm to 1 mΩ.cm. The improvement factor is of 3.4 ("annealed" arrow). Thus, the doping efficiency is two times better for an annealed than a pristine yarn. Reducing the number of CNT defects by annealing treatment make the doping a lot more efficient. As shown in section 3.1, the doping efficiency can be characterized by the reduced activation energy above 70 K. When the annealed CNT yarn is doped, its reduced activation energy is strongly decreased and becomes similar to that of the doped not annealed yarn (see Figure 9b). Even if undoped annealed and pristine yarns have two very distinct electrical transport behavior, when doped, their reduced

activation energy (W) become similar. We therefore experimentally show that the increase of CNT defects largely changes the CNT yarn electrical transport. These results might be explained with the density of state diagrams of Figure 10. Before annealing, (Figure 10a), localized gap state density (traps) $N_t(E)$ are induced by CNT defects. As explained in [55]: "*Anderson localization* [58] *is clearly favored by a disordered defect potential and also by the filamentary nature of the electronic states near the Fermi level in a nanotube at the edge of defect-induced metallization*". Thus, when doped, the localized gap states are partially filled by the carriers induced by doping, consequently the Fermi level shift is not very large and the doping efficiency is 1.7 (part of the carriers induces by doping are trapped). After annealing (Figure 10b), the defect density largely decreases (as stated with the Raman spectroscopy) and consequently the localized gap states density decreases. With the same amount of doping species the Fermi level is now able to move closer to the valence band and thus a better doping efficiency 3.4 is measured. The charge neutrality equation in the material is:

$$Q^+ + p \;=\; N_A^- \;\; with\; Q^+ = q\int_E \; N_t(E)\, f\left(\frac{E - E_F}{kT}\right) dE \;\; and \;\; p = N_V \; \exp\left(\frac{E_V - E_F}{kT}\right) \qquad (3)$$

in the pristine case with N_A^- the density of ionized doping species, Q^+ the density of trapped carriers, p the carrier density and f the Fermi Dirac function while it is just:

$$p = N_A^- \qquad (4)$$

in the annealing case with the assumption that there is no more localized state .

This interpretation is supported by Azadi et al. [59] who calculated that CNT defects induced a density of state increase close to the band edges in the CNT semiconducting bandgap. Furthermore, our experiment also shows that, CNT defects prevent the CNT yarn from reaching high electrical performances and having a good doping efficiency. Our results are also in good agreement with Grujicic et al. [60] who calculated that a perfect CNT has a better O_2 doping efficiency than a defective one.

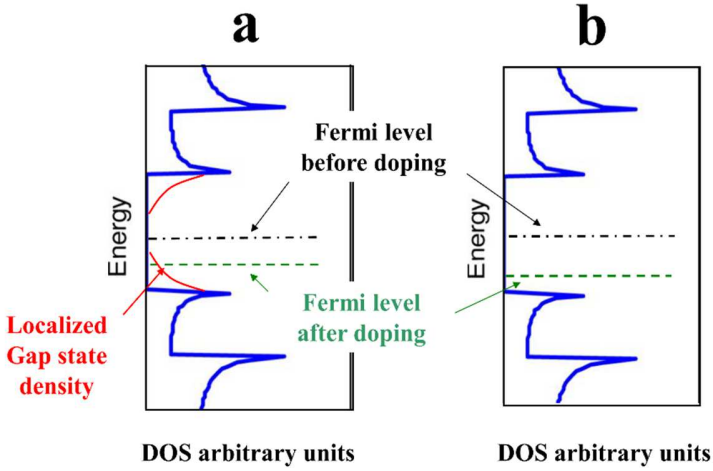

Figure 10: Doped semiconducting CNT density of state with defects (a) and without defect (b)

3.4 Electrical transport scheme for CNT materials (yarn, web)

CNT theory says that statistically 1/3 of the CNT walls should be metallic. However, CNT yarns spun from CNT array, in this work and in the literature, show a semiconducting electrical transport, i.e. the resistivity decreases with temperature until room temperature. One superficial explanation could be that the poor CNT structural quality induced by growing CNT arrays at low temperature hid the CNT yarn metallic behavior. Despite a large increase in the CNT structural quality by annealing treatment, a stronger semiconducting behavior has been clearly observed in our experiments. Furthermore the better the CNTs are, the stronger the semiconducting character is, which completely rules out this explanation. The metallic behavior systematically observed in CNT yarns made from other techniques either floating catalyst (commercial yarn) or wet spinning [61] (as illustrated Figure 11 a and b) cannot only be explained by the CNT quality.

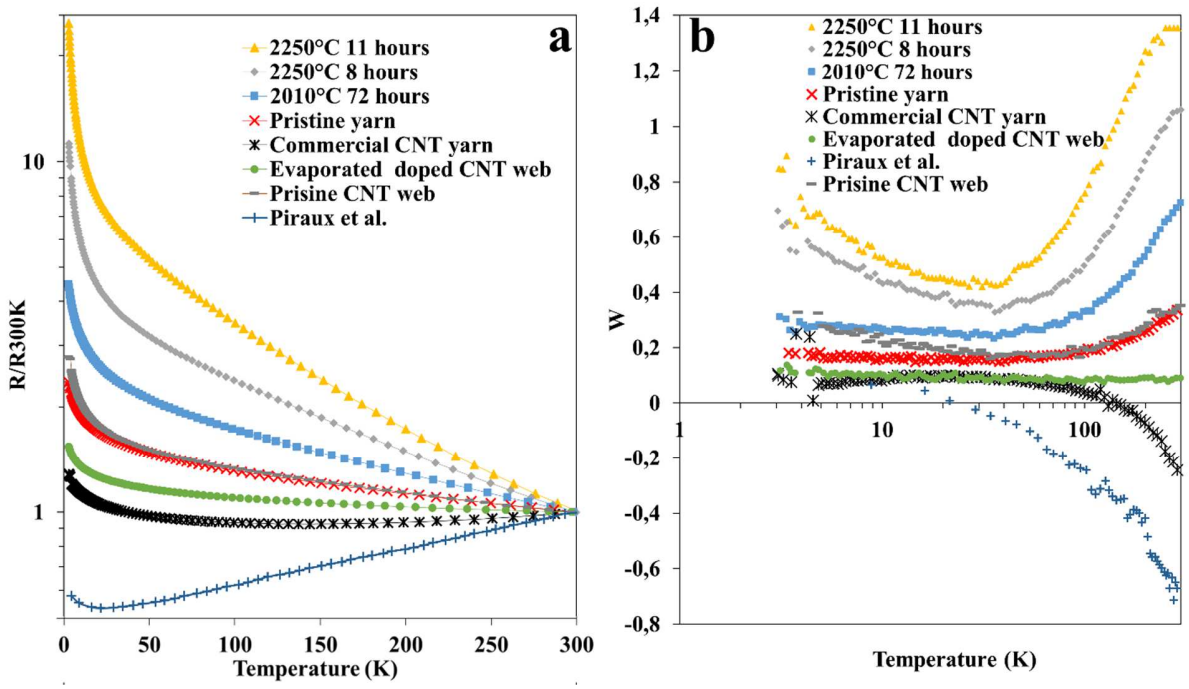

Figure 11: Relative resistance function of the temperature (a) and reduced activation energy (W) function of the temperature (b). Piraux et al. [61].

A strong difference between the CNT yarn elaboration techniques is that CNTs grown in arrays are made of bundles (an average of 7 CNTs per bundle in our case [7]) whereas in the other techniques, CNTs are largely individualized [62]. In this last case, as shown by Xu et al. [63], metallic CNT percolation paths exist in the yarn structure leading to a transport which looks like a metal. On the contrary, due to CNT array growth mechanisms [64], individual CNTs are regrouped into bundles. Considering a Bernoulli distribution, the CNT bundle probability of being metallic is smaller than that of an individual CNT. This probability can be smaller than the threshold of a metallic percolation [62] resulting in the isolation of metallic bundles inside a mainly semiconducting environment. In addition, deformations due to Van der Waals interactions between CNTs inside a bundle induce a band gap opening in metallic CNTs as calculated by Kim et al. [65]. Thus, some CNT bundles inside arrays may have a general semiconducting character. As a consequence, bundles may prevent the existence of a large number of metallic CNT percolation paths in CNT yarns drawn from arrays.

Finally, this work on doping and annealing treatments combined with our previous works [7] on CNT yarn densification and CNT length give us valuable information on the global CNT yarn electronic transport. Analyzing the CNT yarn electronic transport by using the reduced activation energy clearly highlights the different transport mechanism in carbon nanotube materials. We are now able to depict the behavior of the reduced activation energy of CNT yarn and web as function of the temperature (see Figure 12).

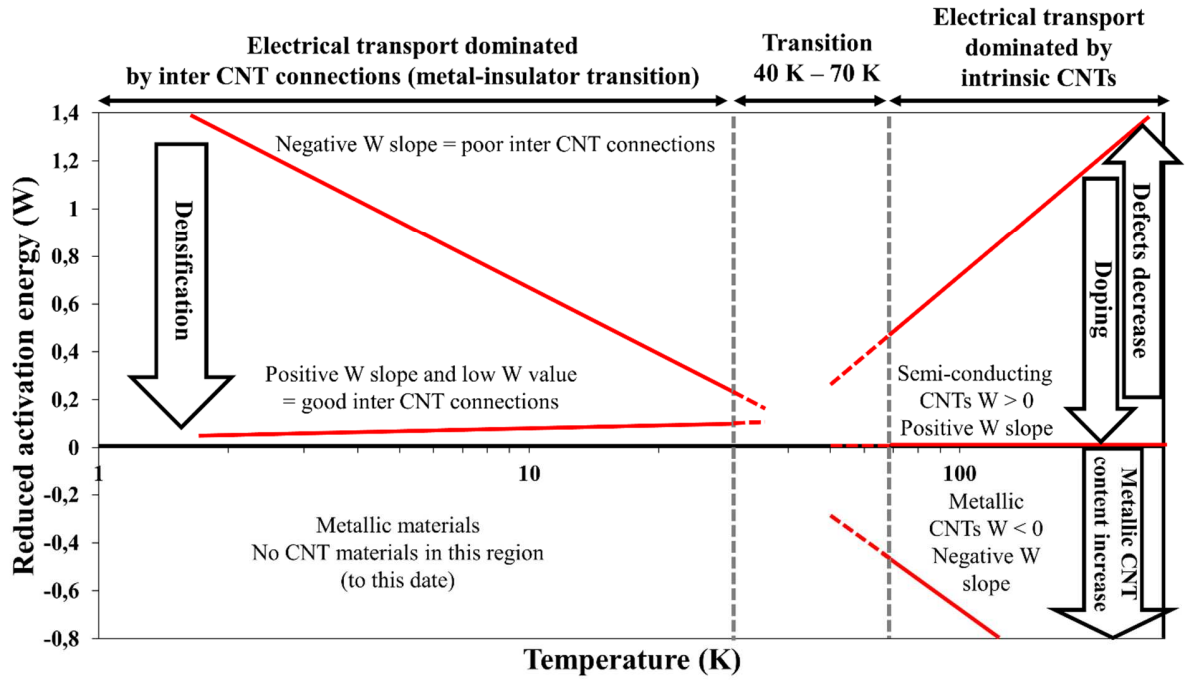

Figure 12: CNT material electrical transport scheme, explaining the shape of the reduced activation energy (W) as a function of the temperature in carbon nanotube yarns and webs

Previously [7], we studied the influence of the CNT yarn density on the CNT yarn electrical transport and concluded that the yarn electrical transport below 70 K (low temperature) is dominated by the inter carbon nanotube connection. We also showed that the intrinsic carbon nanotube electrical transport dominates the electrical transport in yarns above 70 K (high temperature). In general, the lower the W value, the easier the electrical transport. This work clearly shows that modifying the intrinsic CNT electrical transport by doping and annealing treatments changes the W slope above 70 K. In this part, the W slope decreases proportionally to the doping efficiency. The lower the W slope is, the better the doping treatment. Thus, the high temperature analysis of the W slope is a useful and complementary tool to monitor the doping efficiency. The

annealing experiments prove that the number of CNT defects played also a significant role in W slope above 70 K. The diminution of the CNT defects density induces an increase in the W slope above 70 K. Based on the literature [61,66] a negative value of W above 30 K indicates that the CNT yarn electrical transport is dominated by the metallic CNTs. The negative value of the W slope seems also to be correlated to the amount of metallic CNTs [66]. Below 70 K, the CNT yarn electrical transport is governed by the inter CNT connections. This region is well described by the metal-insulator transition. A positive W slope indicate that the transport is on the metallic side of the metal-insulator regime and a negative slope on the insulator side. When the W slope is close to zero it is called the critical regime. In this region the W slope can be tuned by changing the CNT yarn density. All the literature including our work does not report negative W value at very low temperature (below 30 K). This graphic scheme (Figure 12) summarize the electrical transport in carbon nanotube materials (yarn, web). Our analysis can be extended to other type of CNT materials such as network [10], sheets [67] and CNT/polymer composite [68].

4 Conclusion

High temperature annealing (above 2000°C) of CNT yarn spun from CNT arrays drastically reduces the defect density of the tubes as clearly assessed by the Raman spectra and by the factor of 10 increase of the I_G/I_D ratio. Unexpectedly, this improvement increases the semi conducting behaviors of the resistance versus temperature of the yarns and doesn't allow to observe the metallic behavior typical of yarns made by floating catalyst CVD growth process. We think that this result is intrinsic and might be explained by the tubes arrangement in bundles in the case of spun yarn. The annealed CNT yarn resistivity measured in room conditions decreases linearly with the increase of the I_G/I_D ratio characteristic of the CNT structural quality. The CNT yarn resistivity drop from 1.6 mΩ.cm to 0.76 mΩ.cm after annealing. This resistivity value is a new world record resistivity for an undoped CNT yarn spun from CNT array. In addition, we reveal that a good CNT structural quality is not the only parameter needed to reach high conductivities. By doping the CNTs with a new efficient and stable dopant $PtCl_4$, a decrease of the CNT web resistivity at room temperature by a factor of 2.8 is obtained when the dopant solution is deposited by drop casting. Furthermore, a two times higher doping efficiency is demonstrated when the CNT yarn is annealed beforehand. It proves that CNT defects deteriorate the doping efficiency and prevent a good

electrical transport inside CNTs and thus in CNT yarn. The electrical transport analysis of the doped CNT yarn revealed that, above 70 K, the reduced activation energy (W) slope is proportional to the doping improvement factor. The W slope above 70 K can be used to monitor the efficiency of a doping treatment. Thanks to systematic studies of the CNT materials electrical transport, we are now able to depict the influences of many parameters such as CNT length, yarn compaction, doping and annealing treatment on the global CNT yarn electrical transport.

5 Acknowledgment

Thanks are due to Dr. Hélène Le Poche, Dr. Raphaël Ramos and Adeline Fournier for very helpful discussions. Thanks are due for Dr. Hanako Okuno for graphene TEM images. Thanks are due to the Commissariat à l'énergie atomique for PhD funding.

6 References

[1] J. Di, X. Zhang, Z. Yong, Y. Zhang, D. Li, R. Li, Q. Li, Carbon-Nanotube Fibers for Wearable Devices and Smart Textiles, Adv. Mater. 28 (2016) 10529–10538. doi:10.1002/adma.201601186.

[2] Z. Li, Z. Liu, H. Sun, C. Gao, Superstructured Assembly of Nanocarbons: Fullerenes, Nanotubes, and Graphene, Chem. Rev. 115 (2015) 7046–7117. doi:10.1021/acs.chemrev.5b00102.

[3] A. Lekawa-Raus, J. Patmore, L. Kurzepa, J. Bulmer, K. Koziol, Electrical Properties of Carbon Nanotube Based Fibers and Their Future Use in Electrical Wiring, Adv. Funct. Mater. 24 (2014) 3661–3682. doi:10.1002/adfm.201303716.

[4] T.W. Ebbesen, H.J. Lezec, H. Hiura, J.W. Bennett, H.F. Ghaemi, T. Thio, Electrical conductivity of individual carbon nanotubes, Nature. 382 (1996) 54–56. doi:10.1038/382054a0.

[5] A. Todri-Sanial, J. Dijon, A. Maffucci, eds., Carbon Nanotubes for Interconnects: Process, Design and Applications, Springer International Publishing, 2017. //www.springer.com/in/book/9783319297446 (accessed May 15, 2018).

[6] P. Jarosz, C. Schauerman, J. Alvarenga, B. Moses, T. Mastrangelo, R. Raffaelle, R. Ridgley, B. Landi, Carbon nanotube wires and cables: Near-term applications and future perspectives, Nanoscale. 3 (2011) 4542. doi:10.1039/c1nr10814j.

[7] Y. Dini, J. Faure-Vincent, J. Dijon, How to overcome the electrical conductivity limitation of carbon nanotube yarns drawn from carbon nanotube arrays, Carbon. 144 (2019) 301–311. doi:10.1016/j.carbon.2018.12.041.

[8] J.-L. Xu, R.-X. Dai, Y. Xin, Y.-L. Sun, X. Li, Y.-X. Yu, L. Xiang, D. Xie, S.-D. Wang, T.-L. Ren, Efficient and Reversible Electron Doping of Semiconductor-Enriched Single-Walled Carbon Nanotubes by Using Decamethylcobaltocene, Sci. Rep. 7 (2017) 6751. doi:10.1038/s41598-017-05967-w.
[9] S.M. Kim, K.K. Kim, Y.W. Jo, M.H. Park, S.J. Chae, D.L. Duong, C.W. Yang, J. Kong, Y.H. Lee, Role of Anions in the $AuCl_3$ -Doping of Carbon Nanotubes, ACS Nano. 5 (2011) 1236–1242. doi:10.1021/nn1028532.
[10] A.A. Tonkikh, V.I. Tsebro, E.A. Obraztsova, K. Suenaga, H. Kataura, A.G. Nasibulin, E.I. Kauppinen, E.D. Obraztsova, Metallization of single-wall carbon nanotube thin films induced by gas phase iodination, Carbon. 94 (2015) 768–774. doi:10.1016/j.carbon.2015.07.062.
[11] L. Qiu, X. Wang, D. Tang, X. Zheng, P.M. Norris, D. Wen, J. Zhao, X. Zhang, Q. Li, Functionalization and densification of inter-bundle interfaces for improvement in electrical and thermal transport of carbon nanotube fibers, Carbon. 105 (2016) 248–259. doi:10.1016/j.carbon.2016.04.043.
[12] K. Wang, M. Li, Y.-N. Liu, Y. Gu, Q. Li, Z. Zhang, Effect of acidification conditions on the properties of carbon nanotube fibers, Appl. Surf. Sci. 292 (2014) 469–474. doi:10.1016/j.apsusc.2013.11.162.
[13] F. Meng, J. Zhao, Y. Ye, X. Zhang, Q. Li, Carbon nanotube fibers for electrochemical applications: effect of enhanced interfaces by an acid treatment, Nanoscale. 4 (2012) 7464. doi:10.1039/c2nr32332j.
[14] S. Zhang, J.G. Park, N. Nguyen, C. Jolowsky, A. Hao, R. Liang, Ultra-high conductivity and metallic conduction mechanism of scale-up continuous carbon nanotube sheets by mechanical stretching and stable chemical doping, Carbon. 125 (2017) 649–658. doi:10.1016/j.carbon.2017.09.089.
[15] B.P. Gorshunov, E.S. Zhukova, J.S. Starovatykh, M.A. Belyanchikov, A.K. Grebenko, A.V. Bubis, V.I. Tsebro, A.A. Tonkikh, D.V. Rybkovskiy, A.G. Nasibulin, E.I. Kauppinen, E.D. Obraztsova, Terahertz spectroscopy of charge transport in films of pristine and doped single-wall carbon nanotubes, Carbon. 126 (2018) 544–551. doi:10.1016/j.carbon.2017.10.072.
[16] J. Zhao, Q. Li, B. Gao, X. Wang, J. Zou, S. Cong, X. Zhang, Z. Pan, Q. Li, Vibration-assisted infiltration of nano-compounds to strengthen and functionalize carbon nanotube fibers, Carbon. 101 (2016) 114–119. doi:10.1016/j.carbon.2016.01.085.
[17] I. Puchades, C.C. Lawlor, C.M. Schauerman, A.R. Bucossi, J.E. Rossi, N.D. Cox, B.J. Landi, Mechanism of chemical doping in electronic-type-separated single wall carbon nanotubes towards high electrical conductivity, J. Mater. Chem. C. 3 (2015) 10256–10266. doi:10.1039/C5TC02053K.
[18] K.C. Kwon, B.J. Kim, J.-L. Lee, S.Y. Kim, Effect of anions in Au complexes on doping and degradation of graphene, J. Mater. Chem. C. 1 (2013) 2463–2469. doi:10.1039/C3TC00046J.
[19] J. Liang, R. Ramos, J. Dijon, H. Okuno, D. Kalita, D. Renaud, J. Lee, V.P. Georgiev, S. Berrada, T. Sadi, A. Asenov, B. Uhlig, K. Lilienthal, A. Dhavamani, F. Könemann, B. Gotsmann, G. Goncalves, B. Chen, K. Teo, R.R. Pandey, A. Todri-Sanial, A physics-based investigation of Pt-salt doped carbon nanotubes for local interconnects, in: 2017 IEEE Int. Electron Devices Meet. IEDM, 2017: p. 35.5.1-35.5.4. doi:10.1109/IEDM.2017.8268502.

[20] D. Mattia, M.P. Rossi, B.M. Kim, G. Korneva, H.H. Bau, Y. Gogotsi, Effect of Graphitization on the Wettability and Electrical Conductivity of CVD-Carbon Nanotubes and Films, J. Phys. Chem. B. 110 (2006) 9850–9855. doi:10.1021/jp061138s.
[21] Z. Yang, X. Sun, X. Chen, Z. Yong, G. Xu, R. He, Z. An, Q. Li, H. Peng, Dependence of structures and properties of carbon nanotube fibers on heating treatment, J. Mater. Chem. 21 (2011) 13772. doi:10.1039/c1jm12346g.
[22] G. Yamamoto, K. Shirasu, Y. Nozaka, Y. Sato, T. Takagi, T. Hashida, Structure–property relationships in thermally-annealed multi-walled carbon nanotubes, Carbon. 66 (2014) 219–226. doi:10.1016/j.carbon.2013.08.061.
[23] F.Y. Meng, S.Q. Shi, D.S. Xu, C.T. Chan, Surface reconstructions and stability of X-shaped carbon nanotube junction, J. Chem. Phys. 124 (2006) 024711. doi:10.1063/1.2150210.
[24] J.F. Niven, M.B. Johnson, S.M. Juckes, M.A. White, N.T. Alvarez, V. Shanov, Influence of annealing on thermal and electrical properties of carbon nanotube yarns, Carbon. 99 (2016) 485–490. doi:10.1016/j.carbon.2015.12.014.
[25] Dresselhaus M. S., Jorio A., Souza Filho A. G., Saito R., Defect characterization in graphene and carbon nanotubes using Raman spectroscopy, Philos. Trans. R. Soc. Math. Phys. Eng. Sci. 368 (2010) 5355–5377. doi:10.1098/rsta.2010.0213.
[26] R. E. Taylor, H. Groot, Thermophysical Properties of POCO Graphite, High Temp. - High Press. 12 (1978) 34.
[27] A. Zabrodskii, K. Zinoveva, Low-temperature conductivity and metal–insulator transition in compensate n-Ge, Zh Eksp Teor Fiz. 86 (1984) 742.
[28] M. Jouni, J. Faure-Vincent, P. Fedorko, D. Djurado, G. Boiteux, V. Massardier, Charge carrier transport and low electrical percolation threshold in multiwalled carbon nanotube polymer nanocomposites, Carbon. 76 (2014) 10–18. doi:10.1016/j.carbon.2014.04.031.
[29] S.-M. Yoon, U.J. Kim, A. Benayad, I.H. Lee, H. Son, H.-J. Shin, W.M. Choi, Y.H. Lee, Y.W. Jin, E.-H. Lee, S.Y. Lee, J.-Y. Choi, J.M. Kim, Thermal Conversion of Electronic and Electrical Properties of AuCl3-Doped Single-Walled Carbon Nanotubes, ACS Nano. 5 (2011) 1353–1359. doi:10.1021/nn103055u.
[30] K.D. Blauwe, C. Kramberger, W. Plank, H. Kataura, T. Pichler, Raman response of FeCl3 intercalated single-wall carbon nanotubes at high doping, Phys. Status Solidi B. 246 (2009) 2732–2736. doi:10.1002/pssb.200982337.
[31] K. Cui, Y. Qian, I. Jeon, A. Anisimov, Y. Matsuo, E.I. Kauppinen, S. Maruyama, Scalable and Solid-State Redox Functionalization of Transparent Single-Walled Carbon Nanotube Films for Highly Efficient and Stable Solar Cells, Adv. Energy Mater. 7 (2017) 1700449. doi:10.1002/aenm.201700449.
[32] J. Liang, R. Chen, R. Ramos, J. Lee, H. Okuno, D. Kalita, V. Georgiev, S. Berrada, T. Sadi, B. Uhlig, K. Lilienthal, A. Dhavamani, F. Könemann, B. Gotsmann, G. Goncalves, B. Chen, A. Asenov, J. Dijon, A. Todri-Sanial, Investigation of Pt-Salt-Doped-Standalone-Multiwall Carbon Nanotubes for On-Chip Interconnect Applications, IEEE Trans. Electron Devices. 66 (2019) 2346–2352. doi:10.1109/TED.2019.2901658.
[33] A. Das, S. Pisana, B. Chakraborty, S. Piscanec, S.K. Saha, U.V. Waghmare, K.S. Novoselov, H.R. Krishnamurthy, A.K. Geim, A.C. Ferrari, A.K. Sood, Monitoring dopants by Raman scattering in an electrochemically top-gated graphene transistor, Nat. Nanotechnol. 3 (2008) 210–215. doi:10.1038/nnano.2008.67.

[34] L. Yu, T. Grace, M. Batmunkh, M. Dadkhah, C. Shearer, J. Shapter, Insights into chemical doping to engineer the carbon nanotube/silicon photovoltaic heterojunction interface, J. Mater. Chem. A. 5 (2017) 24247–24256. doi:10.1039/C7TA08445E.
[35] J. Chen, J.Y. Shan, T. Tsukada, F. Munekane, A. Kuno, M. Matsuo, T. Hayashi, Y.A. Kim, M. Endo, The structural evolution of thin multi-walled carbon nanotubes during isothermal annealing, Carbon. 45 (2007) 274–280. doi:10.1016/j.carbon.2006.09.028.
[36] J. Di, S. Fang, F.A. Moura, D.S. Galvão, J. Bykova, A. Aliev, M.J. de Andrade, X. Lepró, N. Li, C. Haines, R. Ovalle-Robles, D. Qian, R.H. Baughman, Strong, Twist-Stable Carbon Nanotube Yarns and Muscles by Tension Annealing at Extreme Temperatures, Adv. Mater. 28 (2016) 6598–6605. doi:10.1002/adma.201600628.
[37] A.C. Ferrari, J. Robertson, Interpretation of Raman spectra of disordered and amorphous carbon, Phys. Rev. B. 61 (2000) 14095–14107. doi:10.1103/PhysRevB.61.14095.
[38] L.G. Cançado, A. Jorio, E.H.M. Ferreira, F. Stavale, C.A. Achete, R.B. Capaz, M.V.O. Moutinho, A. Lombardo, T.S. Kulmala, A.C. Ferrari, Quantifying Defects in Graphene via Raman Spectroscopy at Different Excitation Energies, Nano Lett. 11 (2011) 3190–3196. doi:10.1021/nl201432g.
[39] E.F. Antunes, A.O. Lobo, E.J. Corat, V.J. Trava-Airoldi, A.A. Martin, C. Veríssimo, Comparative study of first- and second-order Raman spectra of MWCNT at visible and infrared laser excitation, Carbon. 44 (2006) 2202–2211. doi:10.1016/j.carbon.2006.03.003.
[40] M. Scholz, Y. Hayashi, V. Khavrus, D. Chujo, H. Inoue, M. Hada, A. Leonhardt, B. Büchner, S. Hampel, Resistance-heating of carbon nanotube yarns in different atmospheres, Carbon. 133 (2018) 232–238. doi:10.1016/j.carbon.2018.03.022.
[41] N. Behabtu, C.C. Young, D.E. Tsentalovich, O. Kleinerman, X. Wang, A.W. Ma, E.A. Bengio, R.F. ter Waarbeek, J.J. de Jong, R.E. Hoogerwerf, others, Strong, light, multifunctional fibers of carbon nanotubes with ultrahigh conductivity, Science. 339 (2013) 182–186.
[42] R.J. Headrick, D.E. Tsentalovich, J. Berdegué, E.A. Bengio, L. Liberman, O. Kleinerman, M.S. Lucas, Y. Talmon, M. Pasquali, Structure-Property Relations in Carbon Nanotube Fibers by Downscaling Solution Processing, Adv. Mater. 30 (2018) 1704482. doi:10.1002/adma.201704482.
[43] D.E. Tsentalovich, R.J. Headrick, F. Mirri, J. Hao, N. Behabtu, C.C. Young, M. Pasquali, Influence of Carbon Nanotube Characteristics on Macroscopic Fiber Properties, ACS Appl. Mater. Interfaces. 9 (2017) 36189–36198. doi:10.1021/acsami.7b10968.
[44] S. Suzuki, K. Yamaya, Y. Homma, Y. Kobayashi, Activation energy of healing of low-energy irradiation-induced defects in single-wall carbon nanotubes, Carbon. 48 (2010) 3211–3217. doi:10.1016/j.carbon.2010.05.006.
[45] S. Lee, Y.-C. Liu, C.-H. Chen, Raman study of the temperature-dependence of plasma-induced defect formation rates in carbon nanotubes, Carbon. 50 (2012) 5210–5216. doi:10.1016/j.carbon.2012.07.004.
[46] P. Vinten, P. Marshall, J. Lefebvre, P. Finnie, Thermodynamic and Energetic Effects on the Diameter and Defect Density in Single-Walled Carbon Nanotube Synthesis, J. Phys. Chem. C. 117 (2013) 3527–3536. doi:10.1021/jp308672a.
[47] F. Banhart, J. Kotakoski, A.V. Krasheninnikov, Structural Defects in Graphene, ACS Nano. 5 (2011) 26–41. doi:10.1021/nn102598m.
[48] M. Kabir, K.J. Van Vliet, Kinetics of Topological Stone–Wales Defect Formation in Single-Walled Carbon Nanotubes, J. Phys. Chem. C. 120 (2016) 1989–1993. doi:10.1021/acs.jpcc.5b11682.

[49] L.G. Zhou, S.-Q. Shi, Formation energy of Stone–Wales defects in carbon nanotubes, Appl. Phys. Lett. 83 (2003) 1222–1224. doi:10.1063/1.1599961.
[50] K. Suenaga, H. Wakabayashi, M. Koshino, Y. Sato, K. Urita, S. Iijima, Imaging active topological defects in carbon nanotubes, Nat. Nanotechnol. 2 (2007) 358–360. doi:10.1038/nnano.2007.141.
[51] G.U. Sumanasekera, C.K.W. Adu, S. Fang, P.C. Eklund, Effects of Gas Adsorption and Collisions on Electrical Transport in Single-Walled Carbon Nanotubes, Phys. Rev. Lett. 85 (2000) 1096–1099. doi:10.1103/PhysRevLett.85.1096.
[52] P.G. Collins, K. Bradley, M. Ishigami, A. Zettl, Extreme Oxygen Sensitivity of Electronic Properties of Carbon Nanotubes, Science. 287 (2000) 1801–1804. doi:10.1126/science.287.5459.1801.
[53] A. Lekawa-Raus, L. Kurzepa, G. Kozlowski, S.C. Hopkins, M. Wozniak, D. Lukawski, B.A. Glowacki, K.K. Koziol, Influence of atmospheric water vapour on electrical performance of carbon nanotube fibres, Carbon. 87 (2015) 18–28. doi:10.1016/j.carbon.2015.02.018.
[54] R. Menon, C.O. Yoon, D. Moses, A.J. Heeger, Y. Cao, Transport in polyaniline near the critical regime of the metal-insulator transition, Phys. Rev. B. 48 (1993) 17685.
[55] V.H. Crespi, M.L. Cohen, A. Rubio, In situ band gap engineering of carbon nanotubes, Phys. Rev. Lett. 79 (1997) 2093.
[56] S. Agrawal, M.S. Raghuveer, H. Li, G. Ramanath, Defect-induced electrical conductivity increase in individual multiwalled carbon nanotubes, Appl. Phys. Lett. 90 (2007) 193104. doi:10.1063/1.2737127.
[57] B. Bourlon, C. Miko, L. Forró, D.C. Glattli, A. Bachtold, Determination of the Intershell Conductance in Multiwalled Carbon Nanotubes, Phys. Rev. Lett. 93 (2004) 176806. doi:10.1103/PhysRevLett.93.176806.
[58] P.W. Anderson, Absence of Diffusion in Certain Random Lattices, Phys. Rev. 109 (1958) 1492–1505. doi:10.1103/PhysRev.109.1492.
[59] S. Azadi, R. Moradian, A.M. Shafaee, The effect of Stone-Wales defect orientations on the electronic properties of single-walled carbon nanotubes, Comput. Mater. Sci. 49 (2010) 699–703. doi:10.1016/j.commatsci.2010.06.013.
[60] M. Grujicic, G. Cao, R. Singh, The effect of topological defects and oxygen adsorption on the electronic transport properties of single-walled carbon-nanotubes, Appl. Surf. Sci. 211 (2003) 166–183. doi:10.1016/S0169-4332(03)00224-1.
[61] L. Piraux, F. Abreu Araujo, T.N. Bui, M.J. Otto, J.-P. Issi, Two-dimensional quantum transport in highly conductive carbon nanotube fibers, Phys. Rev. B. 92 (2015) 085428. doi:10.1103/PhysRevB.92.085428.
[62] R.M. Sundaram, K.K.K. Koziol, A.H. Windle, Continuous Direct Spinning of Fibers of Single-Walled Carbon Nanotubes with Metallic Chirality, Adv. Mater. 23 (2011) 5064–5068. doi:10.1002/adma.201102754.
[63] F. Xu, Z. Xu, B.I. Yakobson, Site-percolation threshold of carbon nanotube fibers—Fast inspection of percolation with Markov stochastic theory, Phys. Stat. Mech. Its Appl. 407 (2014) 341–349. doi:10.1016/j.physa.2014.04.013.
[64] M. Bedewy, E.R. Meshot, M.J. Reinker, A.J. Hart, Population Growth Dynamics of Carbon Nanotubes, ACS Nano. 5 (2011) 8974–8989. doi:10.1021/nn203144f.
[65] T. Kim, G. Kim, W.I. Choi, Y.-K. Kwon, J.-M. Zuo, Electrical transport in small bundles of single-walled carbon nanotubes: Intertube interaction and effects of tube deformation, Appl. Phys. Lett. 96 (2010) 173107. doi:10.1063/1.3402768.

[66] A. Lekawa-Raus, K. Walczak, G. Kozlowski, M. Wozniak, S.C. Hopkins, K.K. Koziol, Resistance–temperature dependence in carbon nanotube fibres, Carbon. 84 (2015) 118–123. doi:10.1016/j.carbon.2014.11.062.
[67] J.-H. Pöhls, M.B. Johnson, M.A. White, R. Malik, B. Ruff, C. Jayasinghe, M.J. Schulz, V. Shanov, Physical properties of carbon nanotube sheets drawn from nanotube arrays, Carbon. 50 (2012) 4175–4183. doi:10.1016/j.carbon.2012.04.067.
[68] J. Foroughi, G.M. Spinks, S.R. Ghorbani, M.E. Kozlov, F. Safaei, G. Peleckis, G.G. Wallace, R.H. Baughman, Preparation and characterization of hybrid conducting polymer–carbon nanotube yarn, Nanoscale. 4 (2012) 940–945. doi:10.1039/C2NR11580H.

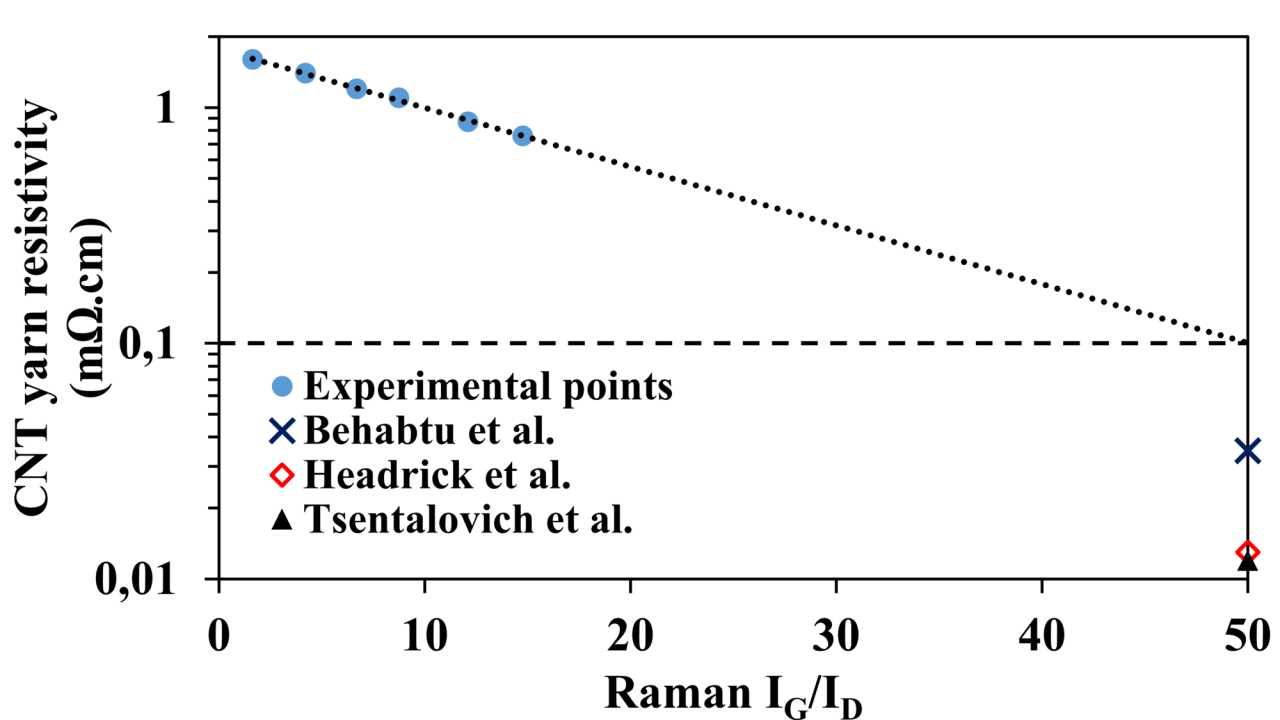
CNT yarn resistivity (mΩ.cm)
1
0,1
0,01
0
10
20
30
40
50
Raman I_G/I_D
Experimental points
Behabtu et al.
Headrick et al.
Tsentalovich et al.